2023

Hypersonic Scramjet Inlet Development for Variable Mach Number Flows

Zachary P. White
University of Central Florida

HYPERSONIC SCRAMJET INLET DEVELOPMENT FOR VARIABLE MACH NUMBER FLOWS

by

ZACHARY PETER WHITE

A thesis submitted in partial fulfillment of the requirements
for the Honors in the Major Program in Aerospace Engineering
in the College of Engineering and Computer Science
and in the Burnett Honors College
at the University of Central Florida
Orlando, Florida

Spring Term, 2023

Thesis Chair: Kareem Ahmed, Ph.D.

ABSTRACT

Hypersonic propulsion has become an increasingly important research field over the past fifty years, and subsequent interest in propulsion systems utilizing supersonic combustion has emerged. Air-breathing engines are desirable for such applications as hypersonic flight vehicles would not need to carry an oxidizer. Therefore, hypersonic air-breathing propulsion systems require an inlet with high mass capture and compressive efficiency. The present work seeks to outline the development and validation of a novel design tool for producing air inlet designs for hypersonic vehicles at variable flight conditions. A Busemann inlet was chosen for its high compressive efficiency, geometric flexibility, and existing experimental validation. The design tool uses the Taylor-Maccoll equation to generate a streamline through a conical flow field. A streamline tracing technique is used to produce three-dimensional inlet surfaces with various capture areas. Additionally, a surface morphing process is implemented to combine inlet profiles for improved engine compatibility. The inlet morphing process allowed for the creation of inlets with offset exit profiles. These offset profiles were evaluated at off-design Mach numbers using three-dimensional viscous simulations to quantify efficiency metrics and characterize starting phenomena.

ACKNOWLEDGEMENTS

I would like to thank my thesis chair Dr. Kareem Ahmed for mentorship and guidance throughout this research and Dr. Michael Kinzel for serving on my thesis committee. I would also like to acknowledge the Naval Research Laboratory for assisting with the numerical simulation of the designs developed in this thesis.

TABLE OF CONTENTS

LIST OF TABLES

LIST OF FIGURES

CHAPTER ONE: BACKGROUND

Introduction

The conceptualization of the supersonic combustion ramjet (scramjet) engine began in the late 1940s and stemmed from a growing interest in the development of hypersonic propulsion systems [1]. As the study of ramjet engines grew near the middle of the twentieth century, researchers began questioning the practicality of ramjet engines exceeding Mach 5 speeds [2, 3]. These concerns influenced international efforts to explore supersonic combustion, and fundamental analysis of scramjet engines demonstrating superior performance above Mach 7 bolstered research interest [1].

Researchers quickly identified various technical challenges that engineers would need to overcome to produce fully operational scramjet designs. The difficulties included characterizing shocks during fuel injection, avoiding thermal choking in the combustor section, and evaluating nozzle performance. Thus, most existing scramjet research focuses on interactions with the combustor [1]. The strong interest in developing a functional scramjet combustor concept has caused researchers to overlook scramjet inlet design generally over the past fifty years [4].

This paper aims to summarize existing research on scramjet inlet design and performance. Due to its geometric flexibility and lack of moving parts, many existing scramjet designs use a Busemann inlet, an internal conical duct that performs adiabatic compression at hypersonic speeds. However, a notable lack of research has been conducted to characterize the performance of such

inlets at off-design Mach numbers which could impact performance immediately after an initial booster stage.

This thesis provides a high-level outline of a novel design tool for Busemann inlets developed by the Propulsion and Energy Research Laboratory at the University of Central Florida. A series of inlets with various capture areas generated using the design tool are also presented. Additionally, an offset exit profile is proposed to mitigate boundary layer effects and improve startability at off-design Mach numbers. The performance of offset Busemann inlets is evaluated using computational fluid dynamics (CFD) at off-design freestream Mach numbers.

Literature Review

Hypersonic Inlet Performance

While not fundamentally differing from the design principles utilized in ramjet engine inlets, scramjet inlets primarily rely on turning from oblique compression waves to compress flow entering the inlet throat and isolator [5]. The reliance on passive compression methods rather than mechanical systems significantly reduces the weight of the engine and the aerodynamic drag through the inlet, making such inlets ideal for hypersonic flight vehicles [6].

The performance of scramjet inlets can be practically evaluated by the amount of compression and total pressure losses during the compression process [7]. A single performance parameter is insufficient to fully characterize a scramjet inlet although some are more useful in evaluating an inlet design. In general, the performance parameters of a scramjet inlet system are determined using flow field properties in the freestream and downstream of the inlet throat [6].

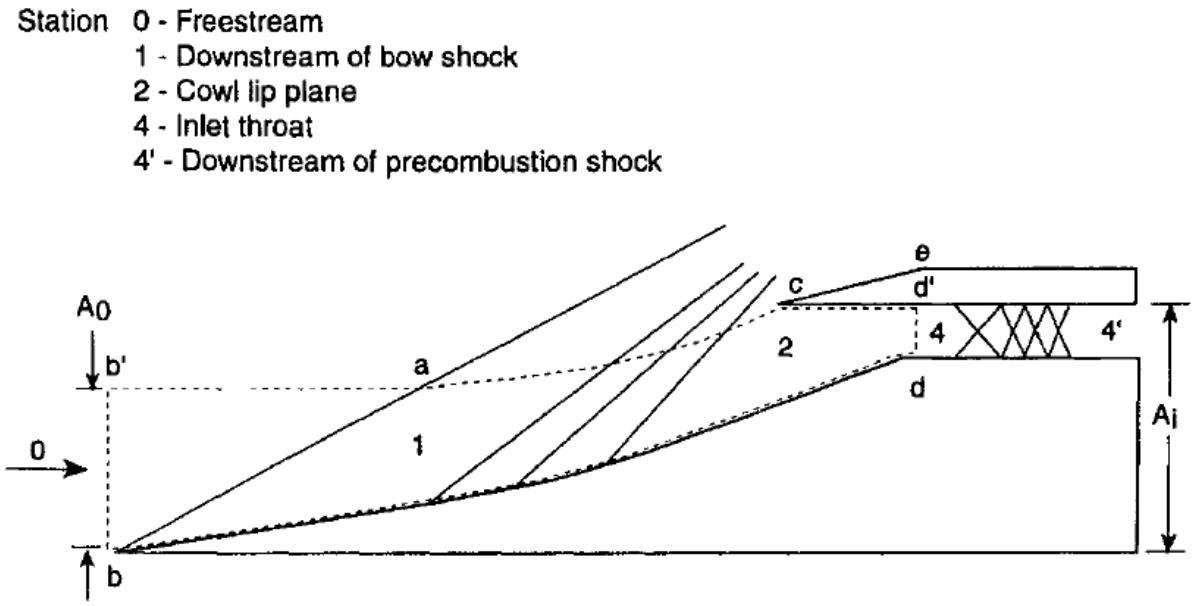

Figure 1: Inlet Station Numbering Convention [6]

Curran and Bergsten [8] define various efficiency parameters for scramjet inlets in terms of flow properties in the freestream and inlet throat, including kinetic energy efficiency, process efficiency, total pressure recovery, static pressure recovery, and polytropic efficiency. Heiser and Pratt [5] characterize those parameters and include an analysis of dimensionless entropy increase in scramjet inlets. Billig and Van Wie [9] continue exploring these parameters and propose additional hypersonic inlet performance analysis metrics. Since these performance parameters are generally obtained from enthalpy values at different thermodynamic states, the compression process of scramjet inlets can be visualized using a Mollier diagram shown in Figure 2.

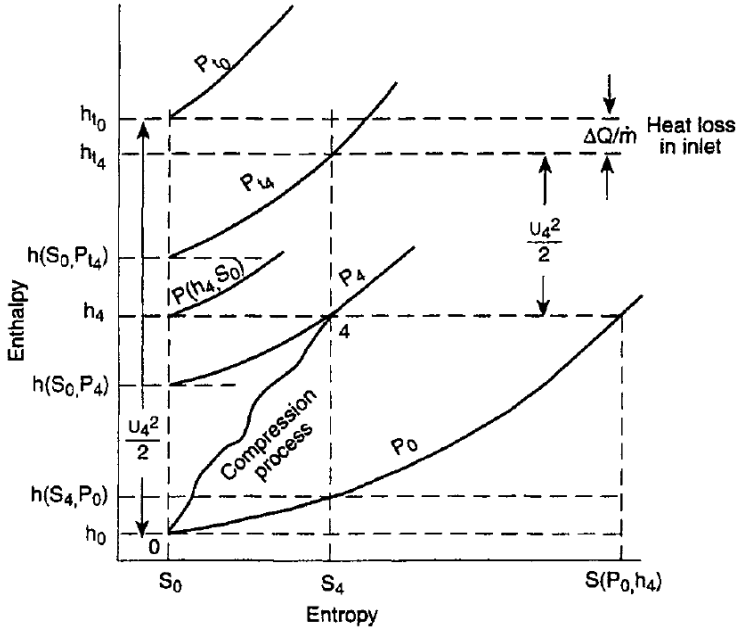

Figure 2: Mollier Diagram for the Inlet Compression Process [6]

Kinetic energy efficiency (η_{KE}) is the ratio of kinetic energy available by isentropic expansion from the inlet exit plane to the initial entrance condition and the freestream kinetic energy [5-6, 8-9]. Curran and Bergsten [8] provide a range of theoretical kinetic energy efficiency values.

$$\left(\frac{V_4}{V_0}\right)^2 < \eta_{KE} < 1 \tag{1}$$

While a usable value of kinetic energy efficiency can be found through various empirical relations, Billig and Van Wie [9] define a generalized relation for real and adiabatic systems.

$$\eta_{KE} = \frac{h_{t_4} - h(P_0, s_4)}{h_{t_0} - h_0} \tag{2}$$

$$\eta_{KE,adiabatic} = \frac{h_{t_0} - h(P_0, s_4)}{h_{t_0} - h_0} \tag{3}$$

Heiser and Pratt [5] provide a relation for kinetic energy efficiency in terms of flow property ratios and Mach number, which can be found more easily from isentropic flow equations. The total pressure ratio (π_c) can be determined through oblique shock relations, and the static temperature ratio (ψ) is found using isentropic flow equations across an oblique shock. Using those property ratios and assuming constant specific heats, a definition of compression efficiency is obtained.

$$\pi_c = \frac{p_{t_4}}{p_{t_0}} \tag{4}$$

$$\psi = \frac{T_4}{T_0} \tag{5}$$

$$\eta_c = \frac{h(P_4, s_0) - h_0}{h_4 - h_0} = \frac{\psi - \pi_c^{-\frac{\gamma-1}{\gamma}}}{\psi - 1} \tag{6}$$

A closed-form equation of kinetic energy efficiency can be found by substituting this relation for compression efficiency.

$$\eta_{KE} = 1 - \frac{2}{(\gamma - 1)M_0^2}(\psi - 1)(1 - \eta_c) \tag{7}$$

To fully characterize inlet performance, the entropy rise through the inlet must be considered [5-6, 8-9]. In general scramjet inlets, entropy rises due to viscous forces in the boundary layer, and some inlets utilize a terminating shock [5]. Quantifying the dimensionless entropy rise allows for further characterization of the thermodynamic efficiency of scramjet inlet designs.

$$\frac{s_4 - s_0}{R} = \frac{\gamma}{\gamma - 1} ln[\psi(1 - \eta_c) + \eta_c] \tag{8}$$

Conical Flow

Conical flow is a specific degenerate three-dimensional (3D) flow over a sharp cone at a zero-degree angle of attack relative to the incoming freestream [10]. Conical flow fields are present in various practical systems such as flow past the fuselage of supersonic aircraft and flow in supersonic nozzles and diffusers [11]. The defining characteristic of conical flow is that flow is axisymmetric, implying that all flow properties remain constant with respect to the azimuthal angle ϕ [10-12].

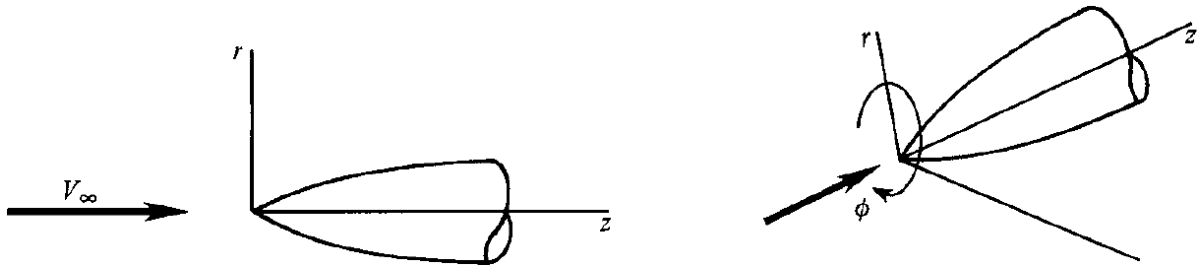

Figure 3: Cylindrical Coordinate System for an Axisymmetric Body [10]

An additional property of conical flow is that flow properties remain constant along a ray from the vertex of the spherical coordinate system. By applying the assumptions of axisymmetric flow, a continuity equation can be derived for conical flow [10, 11].

$$2\rho V_r + \rho V_\theta cot(\theta) + 2\rho \frac{\partial V_\theta}{\partial \theta} + V_\theta \frac{\partial \rho}{\partial \theta} = 0 \tag{9}$$

Furthermore, conical flow is assumed to be steady and isentropic, so the flow field is additionally implied to be irrotational. Applying the axisymmetric flow assumptions to the irrotationality condition produces a relation to determine the angular component of velocity [10-12].

$$V_\theta = \frac{\partial V_r}{\partial \theta} \tag{10}$$

Substituting the previous assumptions into Euler's equations, the Taylor-Maccoll equation can be found [10, 11].

$$\frac{\gamma-1}{2}\left[V_{max}^2 - V_r^2 - \left(\frac{dV_r}{d\theta}\right)^2\right]\left[2V_r + \frac{dV_r}{d\theta}cot\theta + \frac{d^2V_r}{d\theta^2}\right] - \frac{dV_r}{d\theta}\left[V_r\frac{dV_r}{d\theta} + \frac{dV_r}{d\theta}\frac{d^2V_r}{d\theta^2}\right] = 0 \quad (11)$$

$$\frac{a^2}{\gamma-1} + \frac{V^2}{2} = \frac{V_{max}^2}{2} \quad (12)$$

Since no closed-form solution exists for the Taylor-Maccoll equation, Anderson [10] provides a nondimensional form of the Taylor-Maccoll equation to expedite numerical solutions.

$$\frac{\gamma-1}{2}\left[1 - V_r'^2 - \left(\frac{dV_r'}{d\theta}\right)^2\right]\left[2V_r' + \frac{dV_r'}{d\theta}cot\theta + \frac{d^2V_r'}{d\theta^2}\right] - \frac{dV_r'}{d\theta}\left[V_r\frac{dV_r'}{d\theta} + \frac{dV_r'}{d\theta}\frac{d^2V_r'}{d\theta^2}\right] = 0 \quad (13)$$

$$V' = \frac{V}{V_{max}} \quad (14)$$

Alternatively, Thompson [12] determined a first-order equation in terms of the speed of sound to describe conical flow coupled with the axisymmetric irrotationality condition.

$$\frac{dV_\theta}{d\theta} = -V_r + \frac{a^2(V_r + V_\theta cot\theta)}{V_\theta^2 - a^2} \quad (15)$$

Molder [13] recasts the first-order coupled Taylor-Maccoll equation in terms of radial and polar Mach number components labeled *u* and *v*, respectively. Eliminating the speed of sound as a variable reduces computation time to solve the first-order Taylor-Maccoll equations numerically. Additionally, obtaining a Mach number gradient of a conical flow field provides practical physical interpretations of the Taylor-Maccoll equation.

$$\frac{du}{d\theta} = v + \frac{\gamma-1}{2}uv\frac{u + vcot\theta}{v^2 - 1} \quad (16)$$

$$\frac{dv}{d\theta} = -u + \left(1 + \frac{\gamma-1}{2}v^2\right)\frac{u + vcot\theta}{v^2 - 1} \quad (17)$$

Busemann Air Inlets

Busemann [14] theorized the existence of an internal conical flow where fluid is compressed and contracted from the freestream before passing through a terminal conical shock. Courant and Friedrichs [15] explored using Busemann flow within an air intake. Molder and Szpiro [16] used the Taylor-Maccoll equation to generate a hypersonic air inlet employing assumptions of inviscid conical flow.

The Busemann air intake is a converging internal duct that is ideally aligned with the freestream. Because no flow deflection occurs at the leading edge, a conical Mach wave attaches to the leading edge at the freestream Mach angle [13]. Air passes through a series of conical compression waves before a terminating conical shock wave turns the flow back to the freestream direction at the exit. All conical waves and the conical terminal shock are centered at the same origin [13, 16] as shown in the diagram of ideal Busemann flow in Figure 4.

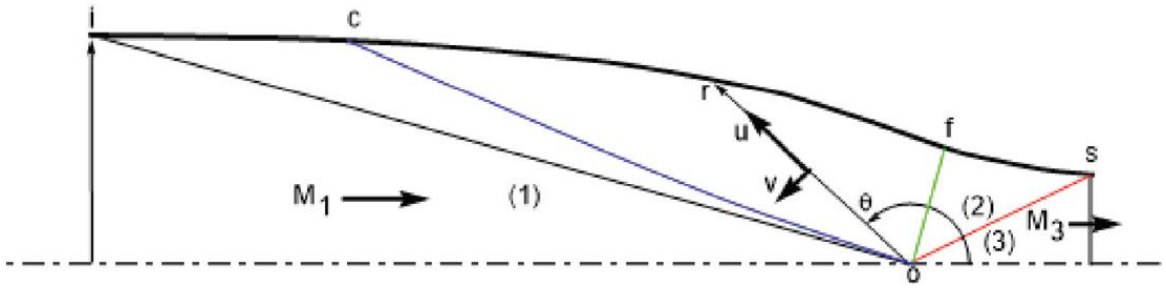

Figure 4: Busemann Inlet Flow Contour [13]

The internal wall contour of Busemann inlets follows a streamline traced through a series of conical compression waves outlined using the Taylor-Maccoll equation. The streamline is determined using a differential equation relating the distance along a vector from the origin of the

Busemann flow field to the radial and angular components of velocity [13]. Assuming flow is isentropic upstream of the conical shock, the radial and angular Mach number components can also be used to define a Busemann streamline.

$$\frac{dr}{d\theta} = r\frac{V_r}{V_\theta} = r\frac{u}{v} \tag{18}$$

A coupled numerical ordinary differential equation (ODE) solver can be implemented to determine a solution Taylor-Maccoll equation and streamline equation when given a Mach number in both the freestream and inlet throat. The initial Mach number components and shock angle for the numerical solution are determined using oblique shock relations for total pressure loss, Mach number, and deflection angle, defined by Equations 19, 20, and 21, respectively [24].

$$\frac{P_{t_4}}{P_{t_0}} = \left[\frac{\frac{\gamma+1}{2}M_0^2 sin^2\theta_s}{1+\frac{\gamma-1}{2}M_0^2 sin^2\theta_s}\right]^{\frac{\gamma}{\gamma-1}} \left[\frac{2\gamma}{\gamma+1}M_0^2 sin^2\theta_s - \frac{\gamma-1}{\gamma+1}\right]^{-\frac{1}{\gamma-1}} \tag{19}$$

$$M_4^2 = \frac{1+\frac{\gamma-1}{2}M_0^2}{\gamma M_0^2 sin^2\theta_s - \frac{\gamma-1}{2}} + \frac{M_0^2 cos^2\theta_s}{1+\frac{\gamma-1}{2}M_0^2 sin^2\theta_s} \tag{20}$$

$$tan\delta = cot\theta\_s\frac{M_0^2 sin^2\theta_s - 1}{\frac{\gamma-1}{2}M_0^2 - (M_0^2 sin^2\theta_s - 1)} \tag{21}$$

The starting angle (θ_2) for integrating the ODE system is found from Equation 22. The system of ODEs is integrated from θ_2 to the freestream Mach angle (μ) defined by Equation 23.

$$\theta_2 = \theta_s - \delta \tag{22}$$

$$\mu = sin^{-1}\left(\frac{1}{M_0}\right) \tag{23}$$

Because the Busemann inlet uses a conical compression flow field, the Mach number distribution is uniform along a ray from the origin of the conical compression system. Figure 5 shows the Mach number distribution within a Busemann inlet, where the top half of the figure is determined using the Taylor-Maccoll equation, and the bottom half is found using CFD.

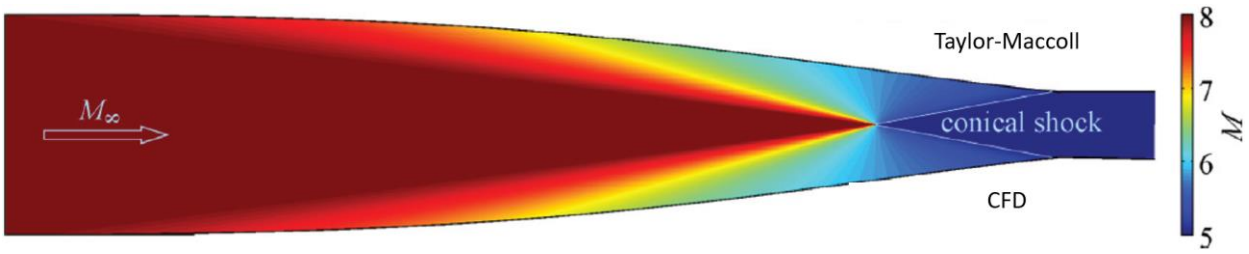

Figure 5: Mach Number Contours of Inviscid Flow through an Axisymmetric Busemann Inlet derived from the Taylor-Maccoll Equation (top half) and CFD (bottom half) [13]

When designing a hypersonic inlet system, the primary design values used for system integration are freestream Mach number, isolator Mach number, and inlet area ratio [13]. Since the solution to the Taylor-Maccoll equation is unknown for a given set of initial conditions prior to generating a numerical solution, the design tool iterates through a series of guess values for total pressure loss and isolator Mach number to determine a unique Busemann streamline for an inlet with desired performance and geometric constraints. However, Busemann streamlines generally produce inlet profiles with high contraction ratios which are unsuitable for hypersonic flight. The starting performance of Busemann inlets must then be considered to determine a viable inlet profile.

Supersonic Inlet Startability Limits

Inlet starting refers to inlet operation such that the internal flow phenomena do not alter inlet capture. Inlets can unstart at sufficiently high contraction ratios or back pressures where flow becomes choked at the inlet throat [18]. Unstarted inlets generally capture less airflow and have lower efficiency than started inlets [6].

The startability range of scramjet inlets is generally bounded by an area ratio theorized by Kantrowitz and Donaldson [18]. This range places a strict limit for potential area ratios that is much lower than the isentropic compression limit used in the design of supersonic nozzles.

$$\left(\frac{A_0}{A_4}\right)_{kantrowitz} = \frac{1}{M_0}\left[\frac{(\gamma+1)M_0^2}{(\gamma-1)M_0^2+2}\right]^{\frac{\gamma}{\gamma-1}}\left[\frac{\gamma+1}{2\gamma M_0^2-(\gamma-1)}\right]^{\frac{1}{\gamma-1}}\left[\frac{1+\gamma-0.5M_0^2}{\gamma+0.5}\right]^{\frac{\gamma+1}{2(\gamma-1)}} \quad (19)$$

$$\left(\frac{A_4}{A_0}\right)_{isentropic} = M_1\left(\frac{\gamma+1}{2}\right)^{\frac{\gamma+1}{2(\gamma-1)}}\left(1+\frac{\gamma-1}{2}M_1^2\right)^{\frac{-(\gamma+1)}{2(\gamma-1)}} \quad (20)$$

However, Smart [19] notes that, although the starting limit developed by Kantrowitz remains a reasonably accurate indicator of two-dimensional (2D) starting phenomena, experimental data compiled by Van Wie et al. [20] and Smart [21] demonstrate that 3D scramjet inlets can start at higher contraction ratios. Molder [22] observes that mass spillage achieved by modifying the inlet capture area or adding of perforation holes can improve startability. Empirical relations developed by Smart [19], Van Wie et al. [20], and Flock and Gulhan [23] provide a more accurate estimation of inlet starting performance. Molder [22] also derives a metric known as the startability index (SI) which is a linear interpolation between the isentropic and Kantrowitz starting limits. He observed that a SI of 0.6 was a sufficient indicator of 3D scramjet inlet starting with mass spillage. The isentropic and Kantrowitz limits as well as a SI=0.6 are shown in Figure 6.

$$SI = \frac{\frac{A_4}{A_0} - \left(\frac{A_4}{A_0}\right)_{isentropic}}{\left(\frac{A_4}{A_0}\right)_{kantrowitz} - \left(\frac{A_4}{A_0}\right)_{isentropic}} \tag{21}$$

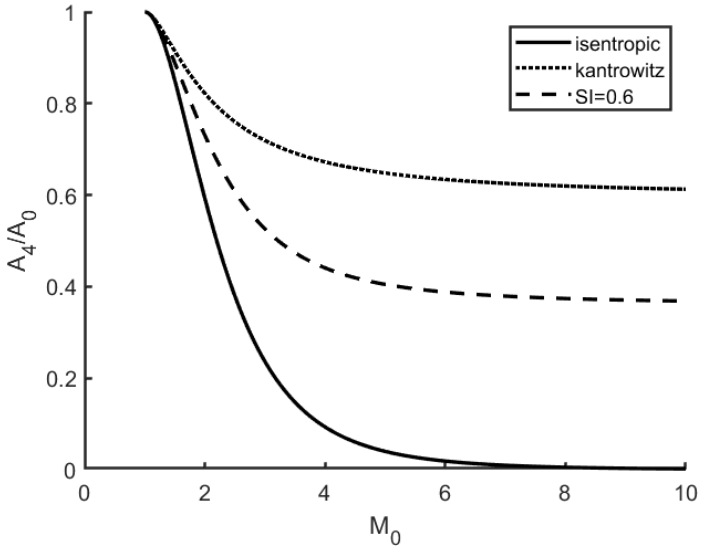

Figure 6: Startability Limits for Scramjet Inlets at Various Freestream Mach Numbers

Streamline Tracing

Streamline tracing is the primary technique used in Busemann inlet design to allow mass spillage at high Mach numbers. Tracing streamlines in a Busemann flow field produces modified inlet designs with improved starting performance. Streamline traced inlets are generally lighter than full Busemann inlets, allowing for greater vehicle compatibility [13].

Billig [24] details the development of SCRAM, an experimental scramjet missile at the Johns Hopkins Applied Physics Laboratory utilizing a modified Busemann inlet profile for improved inlet startability. He refers to the process of modifying inlet profiles as streamline tracing

(also called streamtracing or wavecatching throughout literature). Kothari et al. [25] characterize modified Busemann profiles by introducing a radial deviation parameter (RDP) that describes how much a flow field deviates from a 2D flow. Using the SCRAM inlet as a reference, Billig and Kothari [26] provide a method of generating streamline traced Busemann inlets for general RDP values. The process used to shape the SCRAM inlet is shown in Figure 7. Molder [13] explains a more generalized process for streamline tracing using assumptions of axisymmetric flow.

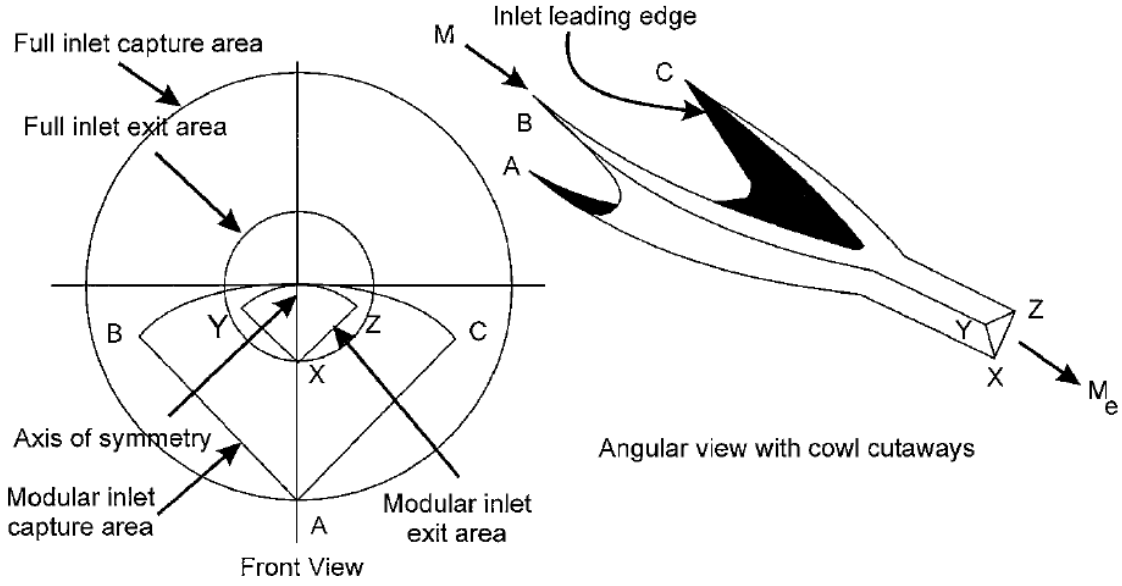

Figure 7: Visualization of Streamline Tracing Technique [26]

A 2D Busemann streamline can be described as a function $r = f(\theta)$. However, Molder [13] explains that a 3D inlet surface can be modified using an additional function $y(\phi)$ that defines the shape of the Busemann inlet capture area as a function of the azimuthal angle. Therefore, the surface of a Busemann inlet in a spherical coordinate system is defined by $r = f(\theta)y(\phi)$. Figure 8 shows a series of streamlines for an inlet with a modified circular capture

area, known as a sugarscoop inlet with $y = -sin(\phi)$. More complex cross-sections can be generated using polar piecewise functions of the azimuthal angle.

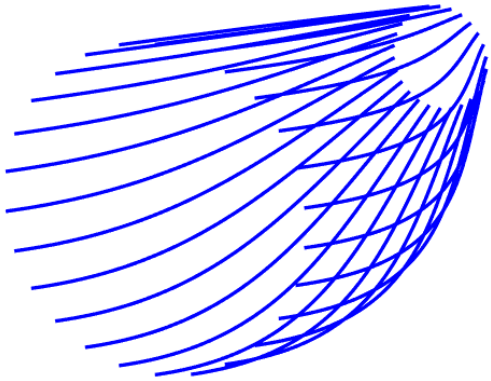

Figure 8: Streamlines for a Sugarscoop Inlet

Taylor and Van Wie [27] introduce a set of functions to morph streamline traced flow fields. Morphing Busemann inlets allows for the specification of a specific shape of the inlet capture and throat areas. The morphing process uses a user-specified function to interpolate between two inlet profiles, and a set of inlet morphing functions are plotted in Figure 9. Morphing Busemann inlet profiles can improve engine compatibility by modifying the flow exit area to a common isolator shape. However, a notable caveat of morphing Busemann inlets is that the flow field is no longer conical. Thus, efficiency and starting data determined from the Taylor-Maccoll equation are not directly applicable [13]. Thus, numerical simulations are necessary to characterize morphed Busemann inlets fully.

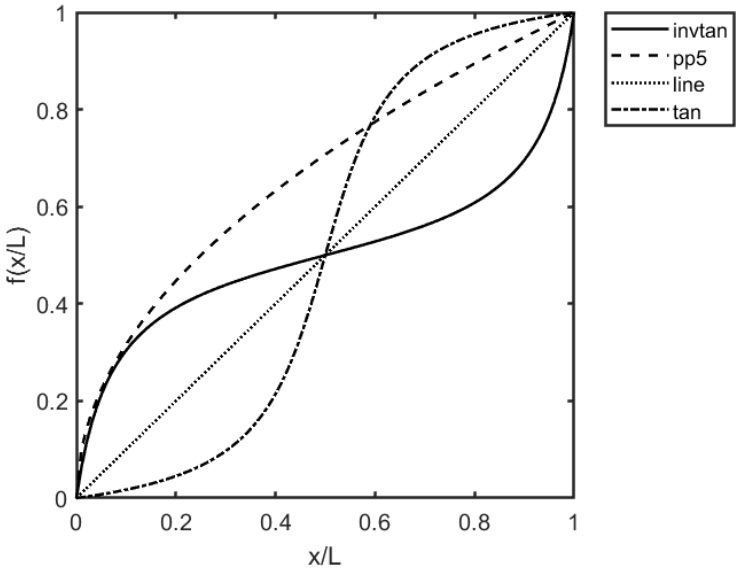

Figure 9: Busemann Inlet Morphing Functions

CHAPTER TWO: METHODOLOGY

Busemann Inlet Design Tool

To generate hypersonic scramjet inlet designs that could be used for numerical simulations and experimental testing, a Busemann inlet design tool was developed using the numerical procedure outlined by Molder [13]. However, many potential concerns with the procedure (most notably time complexity) were addressed to develop a program capable of generating highly accurate 2D Busemann streamlines. The primary issues addressed during the development process were solver tolerance and the runtime cost associated with a high-fidelity solver.

Two numerical methods are called to generate a Busemann streamline. First, a nonlinear quasi-Newton solver is used to determine the initial conditions immediately upstream of the terminating conical shock. After the initial conditions are determined, a coupled Runge-Kutta-Fehlberg (RKF) method is used to solve the system of recast first-order Taylor-Maccoll equations and streamline function. The time complexity of quasi-Newton methods and the RKF are O(n), where $n_{qn} = \frac{\Delta x}{x_{max} - x_{min}}$ and $n_{RKF} = \frac{\Delta t}{t_{max} - t_{min}}$. Therefore, the method proposed by Molder [13] of iterating linearly through guess values of total pressure ratio (where $n_{pt} = \frac{\Delta \pi_c}{\pi_{c_{max}} - \pi_{c_{min}}}$) has a worst-case runtime bounded by Equation 18.

$$f(n) = n_{pt}\left(n_{qn} + n_{RKF}\right) \tag{22}$$

At high values of n_{pt}, $n_{pt} \gg n_{qn} + n_{RKF}$. Therefore, the linear dependence of n_{pt} is the primary factor impacting the runtime of the previous method. The worst-case runtime increases when generating a streamline for an inlet with a specific area ratio. While specifying an area ratio,

the algorithm also linearly iterates through a series of guess values for either the freestream or isolator Mach number. Therefore, the factor n_M must also be considered. Because n_{pt} is generally of a similar order of magnitude compared to n_M, the upper bound for the runtime of the streamline generation algorithm can be described by Equation 19.

$$f(n) = n_{pt} n_M \left(n_{qn} + n_{RKF}\right) \approx n^2 \left(n_{qn} + n_{RKF}\right) \tag{23}$$

The proposed Busemann inlet design tool improves the runtime efficiency of Molder's algorithm without sacrificing the theoretical accuracy of the numerical solution. The improved efficiency of the current design tool allows for significantly faster analysis of inviscid flow field metrics which can be tentatively applied to streamline traced designs.

The design tool was designed in MATLAB and implemented an object-oriented framework to facilitate streamline tracing. The approach allows for improved flexibility in generating streamline traced Busemann inlets allowing for a simplified assessment of Busemann inlet morphology. A series of functions to morph 3D streamline traced Busemann surfaces were also implemented to produce the most generalized set of Busemann inlets possible.

The Busemann inlet design tool can quickly generate Busemann streamlines for a given scramjet engine. These streamlines can be configured for a desired combination of freestream Mach number and isolator Mach number. Figure 10 shows a series of Busemann streamlines for a Mach 6 air freestream with increasing isolator Mach numbers. Area ratio can also be specified, but the resultant isolator Mach number is unknown before a streamline is generated. To evaluate the inlet design tool for generalized Busemann flow fields, contour plots of performance parameters for inviscid Busemann streamlines for a range of Mach number configurations are shown in Figure 11.

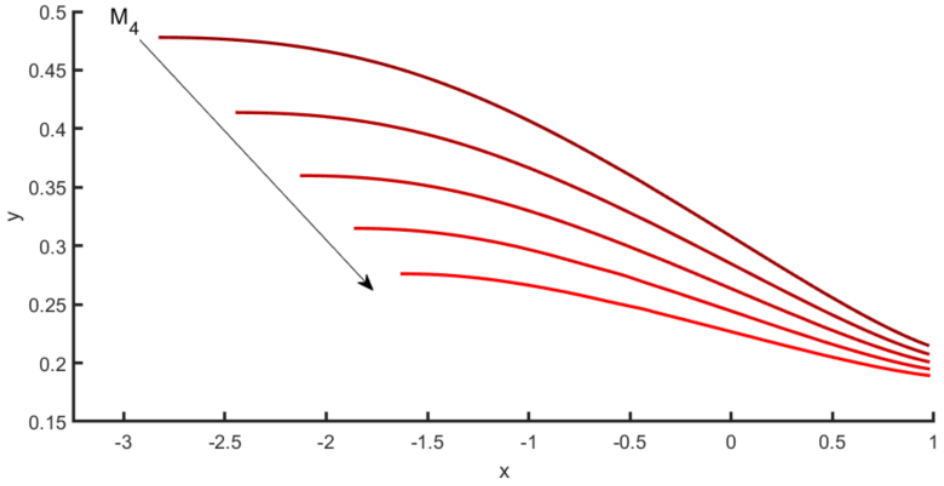

Figure 10: Busemann Streamlines for Increasing Downstream Mach Number

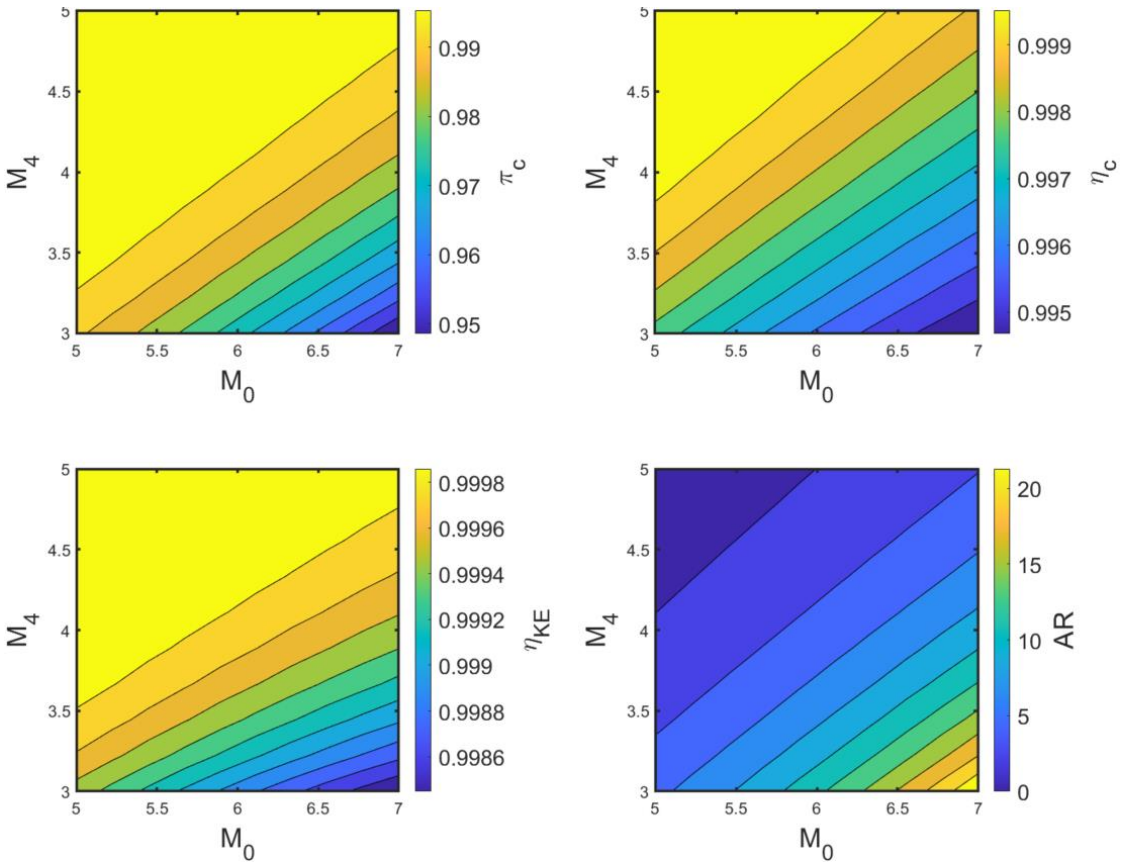

Figure 11: Contour Plots of Total Pressure Ratio, Compression Efficiency, Kinetic Efficiency, and Area Ratio

After a 2D Busemann streamline is generated, a conformal mapping process creates a series of traced streamlines representing a Busemann inlet surface. The design tool incorporates a series of generalized functions in terms of the azimuthal angle. The size and shape of the inlet capture area can be specified before the program is run.

Busemann Inlet Design Procedure

A set of 3D Busemann streamlines were imported as curves into the 3D design software Solidworks where a complete Busemann model is created. First, a series of streamlines are imported as guide curves for the Busemann surface. The surface is subsequently modified with a notch coinciding with the origin of the conical compression waves. The notch is created by revolve cutting the surface of the Busemann inlet with a Mach cone with an angle corresponding to the freestream Mach number. Figure 12 shows the Mach cone used to cut the Busemann Surface, and Figure 13 illustrates the Mach wave that attaches to the leading edge. Cutting a notch in the streamline traced Busemann inlet reduces the weight of the inlet while allowing mass spillage for improved startability.

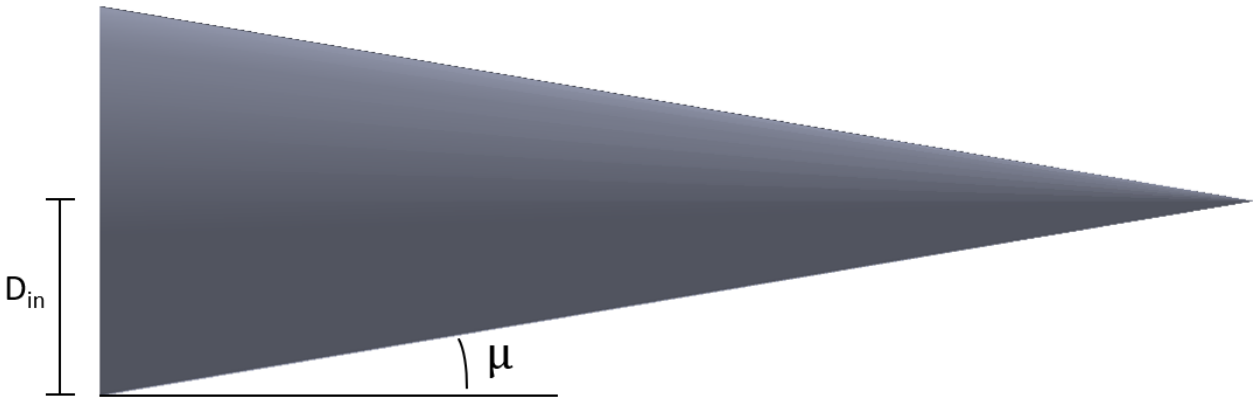

Figure 12: Mach Cone for Creating Busemann Notch

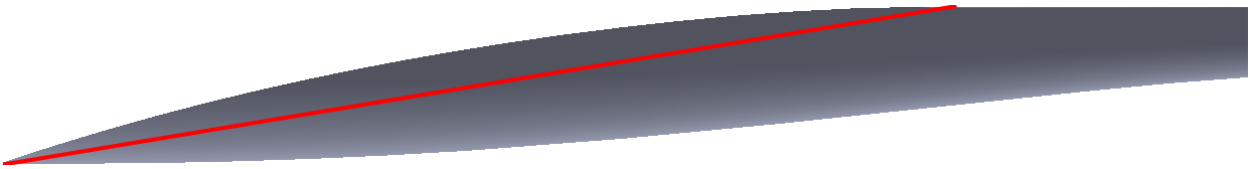

Figure 13: Leading Edge Mach Wave for a Mach 6 Freestream

After surface notching is complete, the Busemann surface is given a uniform thickness to create a solid part. Finally, the outer surface of the Busemann inlet is translated to generate a steep leading edge to reduce the likelihood of a bow shock forming in the freestream.

The Busemann inlets analyzed in this study all featured a capture diameter of 2in and an area ratio of 5. While inlets were created with various capture profiles, the inlets chosen for further evaluation used a sugarscoop design to mitigate potential 3D effects that could occur in other inlet designs.

All Busemann inlets for this report were designed for a Mach 6 air freestream. However, since the flight Mach number will not remain constant throughout operation, an exit offset was implemented to induce starting in a Mach 4 freestream. Multiple offset cross-sections are visualized in Figure 14.

The offset was created using Busemann inlet morphing, so the flow can no longer be accurately assessed using the Taylor-Maccoll equation. Therefore, a three-dimensional numerical simulation was run using Star-CCM+ to evaluate the performance of inlets with different offset distances at a flight Mach number of 4.

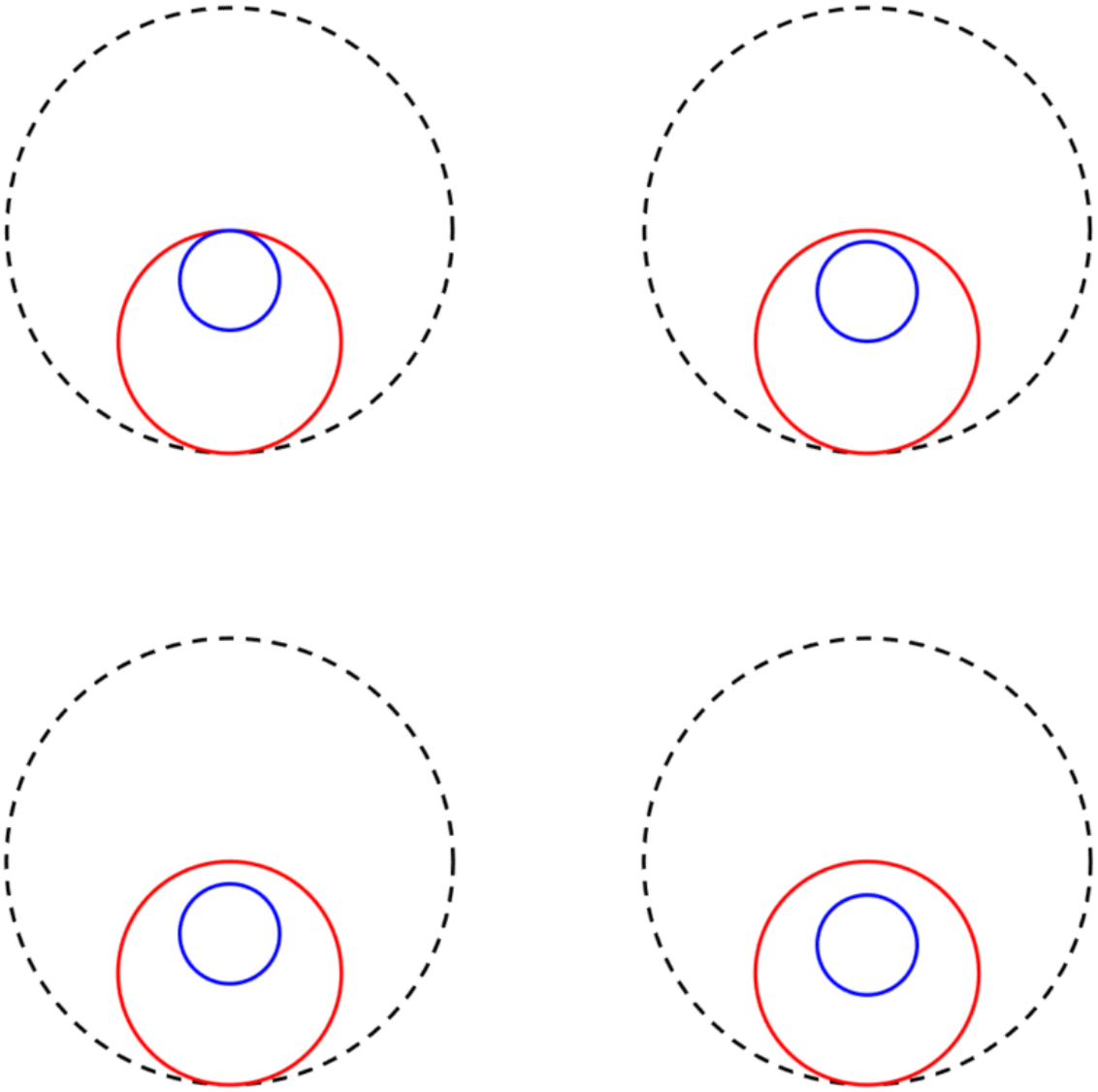

Figure 14: Geometric Busemann Inlet Capture (Red) and Exit (Blue) Profiles for 0%, 5%, 10%, and 15% Offset Exit Profiles

CHAPTER THREE: BUSEMANN INLET DESIGN MORPHOLOGY

Modified Busemann Inlets

The streamline tracing algorithm allows for the creation of Busemann inlets with generalized capture area profiles. While the sugarscoop inlet was the primary design for analysis, additional inlet designs were also generated to assess the effects of streamline tracing. Figure 15 shows the front and isometric views of a sugarscoop inlet. Figures 16, 17, and 18, using the same initial conditions as the sugarscoop inlet, show multiple views of a planar, inward-turning, and outward-turning Busemann inlet.

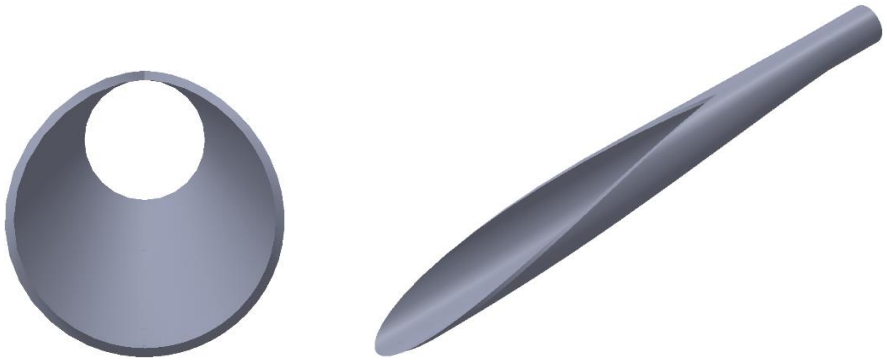

Figure 15: Sugarscoop Busemann Inlet Model Front (left) and Isometric (right) Views

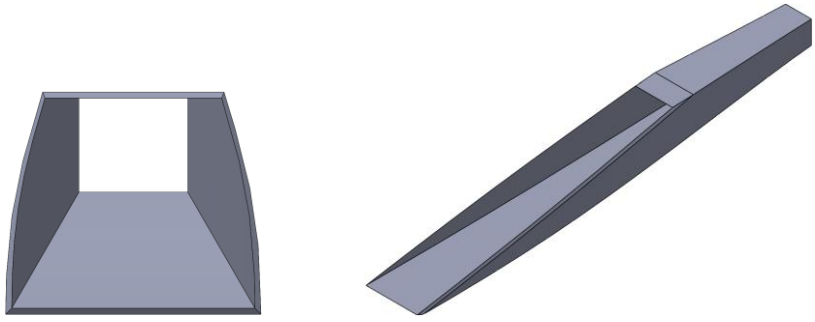

Figure 16: Planar Busemann Inlet Model Front (left) and Isometric (right) Views

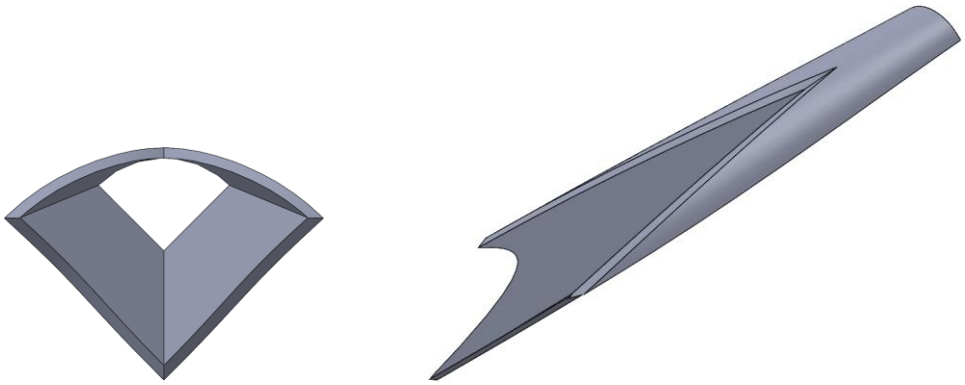

Figure 17: Inward-Turning Busemann Inlet Model Front (left) and Isometric (right) Views

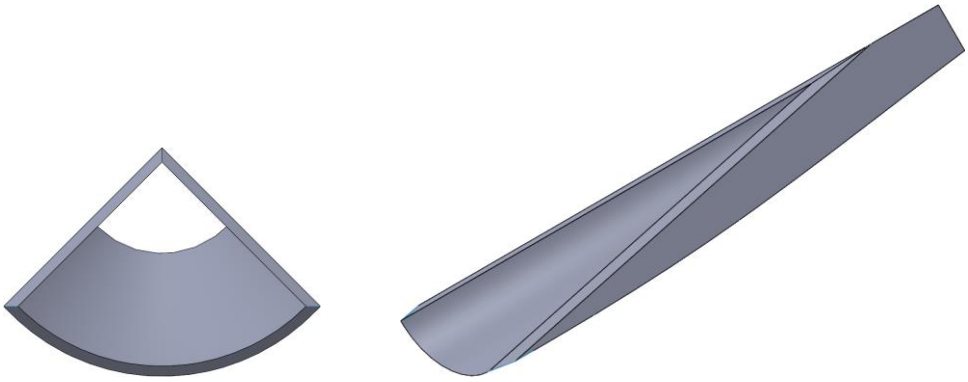

Figure 18: Outward-Turning Busemann Inlet Model Front (left) and isometric (right) views

After creating standard set of streamline traced inlets, the planar inlet was modified with a circular exit profile. The inlet modifications were used to verify the implementation of morphing functions for a 3D surface grid.

One noticeable issue when designing morphed Busemann inlets is of determining a notch location. The primary factor complicating the development of a notch for morphed Busemann inlets is the inapplicability of the Taylor-Maccoll equation. The notch should be located at the origin of the conical compression wave structure since the inlet must swallow an initial bow shock for starting to occur.

Offset Busemann Inlet Profiles

The offset design was produced by morphing two staggered sugarscoop inlet profiles, so a notch location had to be determined for this special case. Figure 19 shows the notch location for the offset inlets where the Mach cone is centered on an axis tangent to the offset exit.

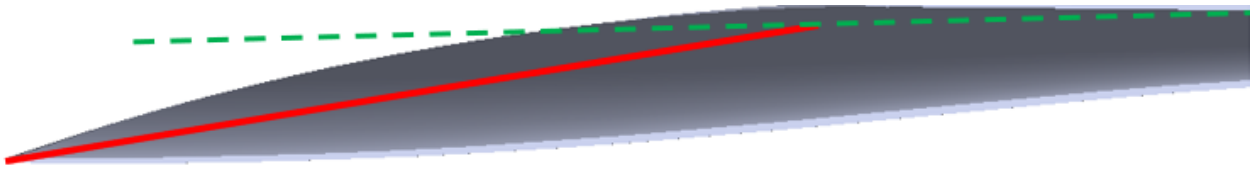

Figure 19: Leading Edge Mach Wave for a Mach 6 Freestream Centered About an Offset Axis

The benefits of a Busemann inlet incorporating an offset exit profile arise from the modified centerline axis and reduced curvature. The most important internal fluid phenomenon inside of a Busemann inlet is the conical terminating shock since it reorients the exit flow to be parallel to the freestream. The terminating shock can be easily characterized in an inviscid flow field, but viscous effects can alter the shock location. The offset inlet could mitigate the effects of the boundary layer on the location of the terminal shock which would improve inlet performance on real flight vehicles.

Depending on the Mach angle chosen for notching the offset Busemann inlet, an opposing terminating shock could form and attach to the wall opposite the leading edge. This opposing terminating shock will produce a more rigid conical shock system, further reducing the impact of the boundary layer. Figure 20 shows how the opposing terminating would attach at different flight Mach numbers.

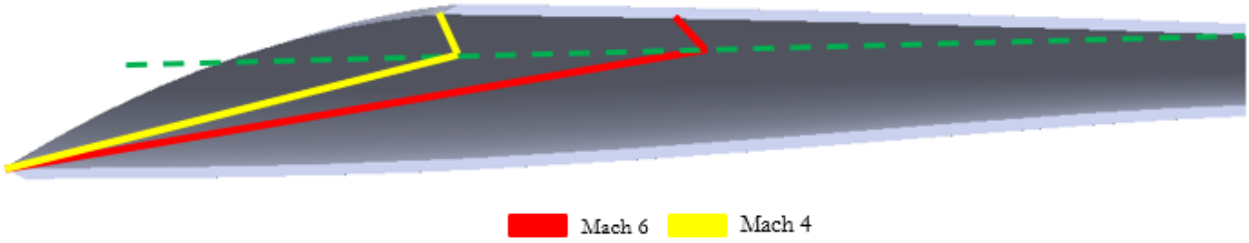

Figure 20: Diagram of an Opposing Terminating Shock at Different Flight Mach Numbers

An additional benefit of a sugarscoop inlet with an offset exit profile is a reduction in mass spillage. Although mass spillage facilitates Busemann inlet starting, the offset profile could provide improved starting performance. The augmented starting capacity would allow a higher air mass flow rate to travel downstream of the inlet, providing increased oxygen for combustion downstream.

Figure 21 shows a Mach number contour of a standard sugarscoop inlet operating in a Mach 4 flow. The supersonic flow in the inlet throat is evidence of inlet starting at an off-design Mach number. Figure 22 also provides evidence of inlet starting in a Mach 4 freestream, implying that both inlets are feasible for flight vehicles operating off-design. However, while Table 1 shows that inlet performance is very similar for both inlet designs, pressure recovery and compression efficiency improved in the offset inlet. As expected, the mass capture increased for the offset case and maintained similar starting characteristics to a sugarscoop inlet.

Although the inlet 5% offset improved overall performance, larger offsets that were simulated produced an unstart condition. Figure 23 and Figure 24 show the formation of a strong shock attached to the inlet cowl with a resultant subsonic flow downstream on the inlet throat. The unstart condition could be a result of decreased mass spillage for larger offsets.

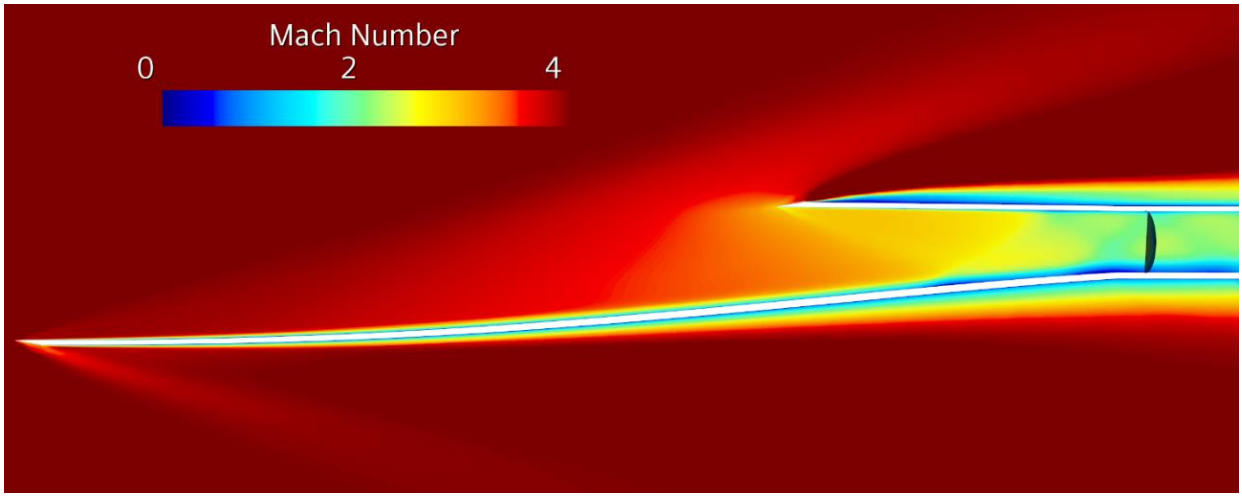

Figure 21: Mach Number Contour of a Sugarscoop Inlet with No Offset in a Mach 4 Freestream

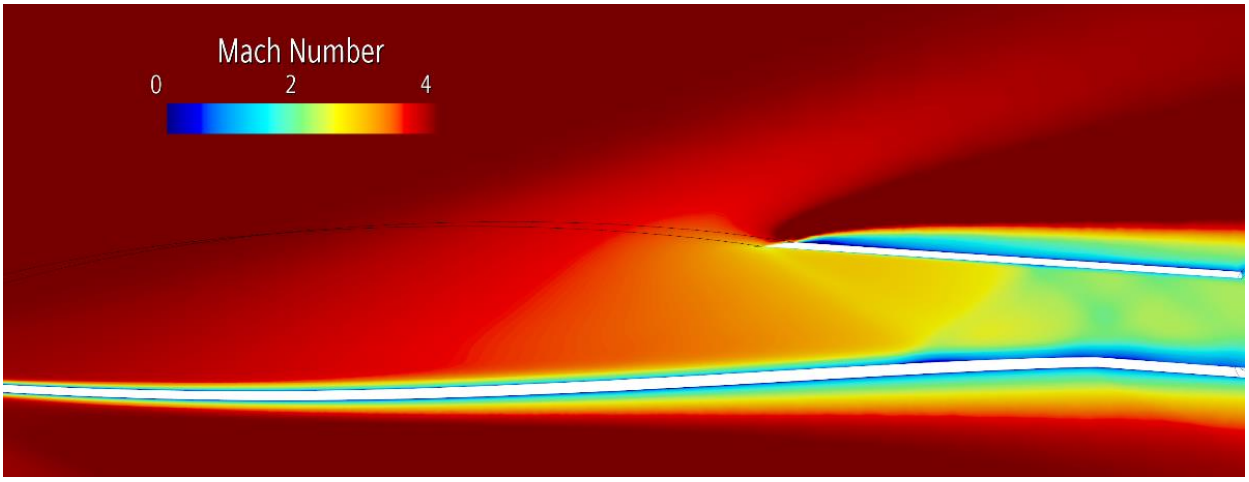

Figure 22: Mach Number Contour of a Sugarscoop Inlet with a 5% Offset in a Mach 4 Freestream

Table 1: Mach 4 Inlet Performance for an Inlet with No Offset and 5% Offset

	M_0	M_4	η_c	Π_{static}	Π_{total}	η_{KE}	$\dot{m}$
Busemann	4	1.54	0.85	17.1	0.59	0.55	0.159
Offset	4	1.52	0.86	18.27	0.60	0.55	0.166

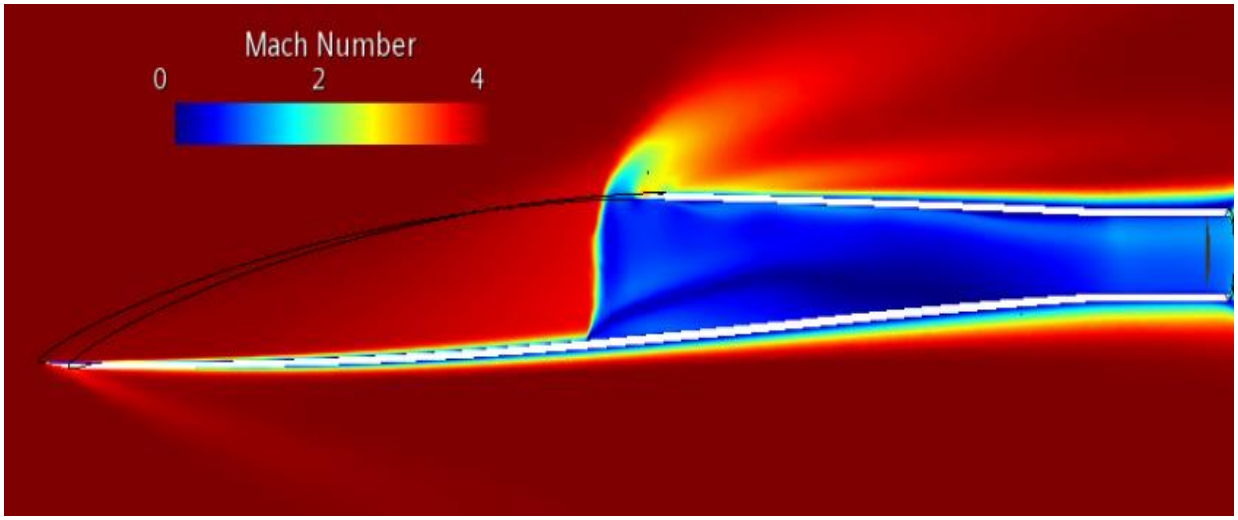

Figure 23: Mach Number Contour of a Sugarscoop Inlet with a 10% Offset in a Mach 4 Freestream

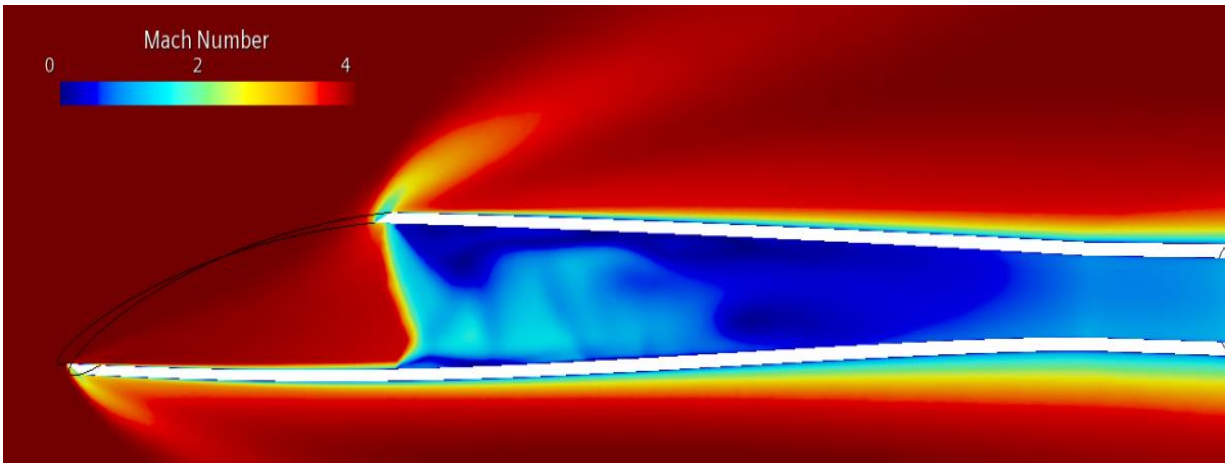

Figure 24: Mach Number Contour of a Sugarscoop Inlet with a 15% Offset in a Mach 4 Freestream

CHAPTER 4: CONCLUSION

A Busemann inlet design tool was developed to generate streamline traced Busemann inlets efficiently. A system of morphing functions was implemented to create offset inlet profiles to aid off-design Mach number performance. The CFD simulations show that a 5% offset inlet was viable for operation at off-design flight Mach numbers. This result suggests the feasibility of an offset Busemann inlet in applications such as dual-mode scramjet engines.

Future work should consider implementing a boundary layer correction model to mitigate viscous effects on the terminating shock. Additionally, a more accurate method of determining the offset origin position would allow for more efficient inlet notching and increased mass capture. Finally, this study did not consider the effects of torque balance nor the performance at different angles of attack.

REFERENCES

[1] Curran, E. T., "Scramjet Engines: The First Forty Years," *Journal of Propulsion and Power*, Vol. 17, No. 6, 2001, pp. 1138-1148.

[2] Mallinson, D. H., "Discussion on Hypersonic Ramjet Development," *High Mach Number Airbreathing* Engines, Pergamon, Oxford, England, U.K., 1961, pp. 80-83.

[3] Hawkins, R., and Fox, M. D., "An Investigation of Real Gas Effects Relevant to the Performance of a Kerosene Fueled Hypersonic Ramjet," *Supersonic Flow, Chemical Processes and Radiative Transfer*, Macmillan, NY, 1964, pp. 113–136.

[4] Curran, E. T., and Murthy, S. N. B., *Scramjet Propulsion*, Progress in Astronautics and Aeronautics, AIAA, Washington, DC, 2001.

[5] Heiser, W. H., Pratt, D. T., Daley, D. H., and Mehta, U. B., "Compression Systems or Components," *Hypersonic Airbreathing Propulsion*, AIAA Education Series, AIAA, Washington, DC, 1994, pp. 197-275.

[6] Van Wie, D. M., "Scramjet Inlets," *Scramjet Propulsion*, Progress in Aeronautics and Astronautics, AIAA, Washington, DC, 2001, pp. 447-511.

[7] Smart, M. K., "Scramjet Inlets," NATO RTO-EN-AVT-185, Sep. 2010.

[8] Curran, E. T., Bergsten, M. B., "Inlet Efficiency Parameters for Supersonic Combustion Ramjet Engines," APL-TDR-64-61, June 1964.

[9] Billig, F. S., and Van Wie, D. M., "Efficiency Parameters for Inlets Operating at Hypersonic Speed," *1987 International Society of Airbreathing Engines Symposium*, June 1987.

[10] Anderson, J. D., "Conical Flow," *Modern Compressible Flow With Historical Perspective*, 3rd ed., McGraw-Hill, New York, 2003, pp. 363-375.

[11] Shapiro, A. H., "Axially Symmetric Supersonic Flow," *The Dynamics and Thermodynamics of Compressible Fluid Flow*, Vol. 2, The Ronald Press Company, 1954, pp. 651-702.

[12] Thompson, P. A., "Self-Similar Motions," *Compressible-Fluid Dynamics*, McGraw-Hill, 1972, pp. 475-516.

[13] Molder, S., "The Busemann Air Intake for Hypersonic Speeds," *Hypersonic Vehicles-Past, Present, and Future Developments*, InTech Open, 2019.

[14] Busemann, A. "Die achsensymmetrische kegelige überschallströmung," Luftfahrtforschung, Vol. 19, No. 4, 1944, pp. 137-144.

[15] Courant, R., Friedrichs, K., "Supersonic Flow and Shock Waves," New York, 1948.

[16] Molder, S., Szpiro, E. J., "Busemann inlet for hypersonic speeds," *Journal of Spacecraft and Rockets*, Vol. 3, No. 8, 1966, pp. 1303-1304.

[17] John, J. E., Keith, T. G., "Oblique Shockwaves," *Gas Dynamics*, Pearson, New Jersey, 2006, pp. 189-228.

[18] Kantrowitz, A., Donaldson, C. "Preliminary Investigation of Supersonic Diffusers," NACA WRL-713, 1945.

[19] Smart, M. K., "How Much Compression Should a Scramjet Inlet Do?," *AIAA Journal*, Vol. 50, No. 3, 2012, pp. 610-619.

[20] Van Wie, D. M, Kwok, F. T., Walsh, R. F., "Starting characteristics of supersonic inlets," AIAA Paper 96-2914, July 1996.

[21] Smart, M. K., "Experimental Testing of a Hypersonic Inlet with Rectangular to Elliptical Shape Transition," *Journal of Propulsion and Power,* Vol. 17, No. 2, 2001, pp. 276-283.

[22] Molder, S., "Flow Starting in High Compression Hypersonic Air Inlets by Mass Spillage," AIAA 2004-4130, July 2004.

[23] Flock, A. K., Gulhan, A., "Modified Kantrowitz Starting Criteria for Mixed Compression Supersonic Intakes," *AIAA Journal*, Vol. 57, No. 5, 2019, pp. 2011-2016.

[24] Billig, F. S., "SCRAM - A Supersonic Combustion Ramjet Missile," *AIAA/SAE/ASME/ASEE Joint Propulsion Conference and Exhibit,* AIAA 93-2329, June 1993.

[25] Kothari, A. P., Tarpley, C., McLaughlin, T. A., Babu, B. S., Livingston, J. W., "Hypersonic vehicle design using inward turning flow fields," AIAA Paper 96-2552, July 1996.

[26] Billig, F. S., Kothari, A. P., "Streamline Tracing: Technique for Designing Hypersonic Vehicles," *Journal of Propulsion and Power,* Vol. 16, No. 3, 2000, pp. 465-471.

[27] Taylor, T. M., Van Wie, D., "Performance Analysis of Hypersonic Shape-Changing Inlets Derived from Morphing Streamline Traced Flowpaths," AIAA 2008-2635, April-May 2008.